Estuarine, Coastal and Shelf Science 231 (2019) 106476

Contents lists available at ScienceDirect

Estuarine, Coastal and Shelf Science

journal homepage: http://www.elsevier.com/locate/ecss

Spatio-temporal variability of natural radioactivity as tracer of beach sedimentary dynamics

A. Arriola-Velásquez, A. Tejera *, J.G. Guerra, I. Alonso, H. Alonso, M.A. Arnedo, J.G. Rubiano, P. Martel

Department of Physics, Instituto Universitario de Investigación en Estudios Ambientales y Recursos Naturales i-UNAT. Universidad de Las Palmas de Gran Canaria, Campus de Tafira, Las Palmas de Gran Canaria, 35017, Spain

ARTICLE INFO

Keywords:
Natural radionuclides
Tracer
Sedimentary processes
Erosion/accretion

ABSTRACT

Knowledge of coastal sedimentary dynamics is an essential tool in the sustainable management of high-value natural places, such as beaches, which play an important role in human life. With this aim, spatio-temporal variations of activity concentrations of the main natural radionuclides in intertidal sand samples were measured in order to analyse their role as tracers of different sedimentary processes on a beach with wide and diversified sedimentary dynamics (Las Canteras beach at Gran Canaria Island). The radionuclides studied were ^{226}Ra, ^{232}Th, ^{40}K and ^{210}Pb$_{ex}$. A cluster analysis and a principal component analysis performed by using stationary averages of the studied radionuclides activity concentrations and other quantities, such as grain size and or bulk density, were developed. These analyses divided the beach into three zones of sediment distribution related to one of the main geomorphological characteristics of the beach. Finally, annual variations in ^{226}Ra/^{228}Ra ratios were used to study erosion and accretion periods on the beach.

1. Introduction

As is known, natural radionuclides include primordial radioactive elements in the earth's crust, their radioactive progeny and cosmogenic radionuclides, which originate in the earth's atmosphere by interaction with cosmic radiation and detected on the earth's surface due to fallout. Naturally occurring radionuclides most commonly found on the earth's crust are primordial nuclides, mainly ^{40}K and the elements from the ^{238}U and ^{232}Th day series. Concentrations of these elements on the earth's surface vary widely from one zone to another depending on their geology as well as other factors such as geochemical and geophysical conditions. The natural radioactivity of a beach is mainly conditioned by the composition of its sands and sediments, which originate from different rocks (with different radionuclide composition) that suffer weathering, erosion and subsequent transport by the action of different agents.

In recent years, numerous assessments of environmental radioactivity (not only of natural origin, but also of anthropogenic ones) have been developed in beach sands and marine sediments from different parts of the world (Abdi et al., 2008; Casas-Ruiz et al., 2012; Fares, 2017; Huang et al., 2015; Korkulu and Özkan, 2013; Malain et al., 2012; Pappa et al., 2016; Shuaibu et al., 2017). In most of these studies, the activity concentrations found for ^{226}Ra (from ^{238}U series decay), ^{232}Th and ^{40}K are on a comparable range among them. However, in some places like Miami Bay in Malaysia (Shuaibu et al., 2017), the northeast coast of Tamilnadu in India (Suresh Gandhi et al., 2014) and Cumuruxatiba Beach in Brazil (Vasconcelos et al., 2011), the activity concentration values are two orders of magnitude higher than in other parts of the world. In fact, in the radiological protection framework, the aim of the aforementioned papers, is radioactive background monitoring of beaches through estimation of radiological exposure to humans due to radionuclides in beach sediments. In this regard, external gamma dose rates and several different radiation hazard indices were estimated in Gran Canaria beaches, and any radiological risks were assessed (Arnedo et al., 2013).

Furthermore, radionuclides in sediments have been used as tracers of different coastal processes including those related to dynamic processes on beaches. For example, ^{238}U, ^{232}Th and ^{40}K have been used as proxy of coastal heavy mineral resources or to estimate biogenic sedimentation (Ghosal et al., 2017; Gulin et al., 2014). Also, particle-reactive radionuclides such as ^{234}Th, ^{210}Pb, ^{7}Be and ^{137}Cs have been used as tracers of sedimentary processes in order to determine sediment transport, sediment accretion/erosion or accumulation and mixing rates (Al-Mur et al.,

* Corresponding author.
E-mail address: alicia.tejera@ulpgc.es (A. Tejera).

https://doi.org/10.1016/j.ecss.2019.106476
Received 30 April 2019; Received in revised form 23 October 2019; Accepted 5 November 2019
Available online 8 November 2019

2017; Carvalho et al., 2016; Du et al., 2010; Mahu et al., 2016; Oguri et al., 2012; Renfro et al., 2016; Woszczyk et al., 2017). It is precisely within this field of application of radionuclides that the aim of the present work is framed.

The main objective of this paper is to analyse the spatial and temporal variability of gamma emitter radionuclides present in the intertidal beach sand in order to study its role as tracers of common sedimentary processes. For this purpose, we have selected a beach (Las Canteras beach in Gran Canaria island) with a diverse sedimentary dynamic, combining the characteristic dynamic of a closed beach with that associated with a beach open to wave action.

2. Study region

Las Canteras beach is one of the most important urban beaches in Spain. It is located in El Confital bay (Medina et al., 2006), an important protected area north of the island of Gran Canaria, in the city of Las Palmas de Gran Canaria (Fig. 1). Las Canteras beach is approximately 3 km long, delimited by La Isleta Isthmus in the north and a breakwater ("Baja de Núñez") in the south. This beach can be divided into three different sectors: the northern arch, the central arch and the southern arch (Fig. 1). Between the central arch and northern arch, there is a smaller sector, "Playa Chica", with physical limitations to the exchange of sediments with the rest of the beach. At high tide periods, tide currents are to the NE, while during low tide periods, they are SW. The wind direction is mainly NE, NNE and ENE due to the trade winds. During spring tides, the tidal range is greater than 2.5 m; during neap tides, it is approximately 1 m. The mean wave approaching direction is north and, during big storms, comes from the northwest. The average significant wave height is 1.42 ± 0.6 m, reaching up to 4 m in winter (Alonso, 1993, 2005).

As described in Alonso (1993), the sediments that compose the beach sand are thought to be provided by the Isleta Isthmus, La Ballena Ravine and the beach rock that can be found in different parts of the beach. Also, they could come from submerged sandbars that are located between the bathymetric curve of 50 m and the beachfront. This work explains that the sand across the beach can be considered medium and fine sands, with a size around 0.25 mm in diameter. The calcimetry and petrographic analysis of Alonso (1993), Alonso and Pérez Torrado (1992) and Medina et al. (2006), show that the lowest amount of organic matter appears on the southern arch of the beach. A geochemical analysis performed on two sand samples from the southern and northern arch,

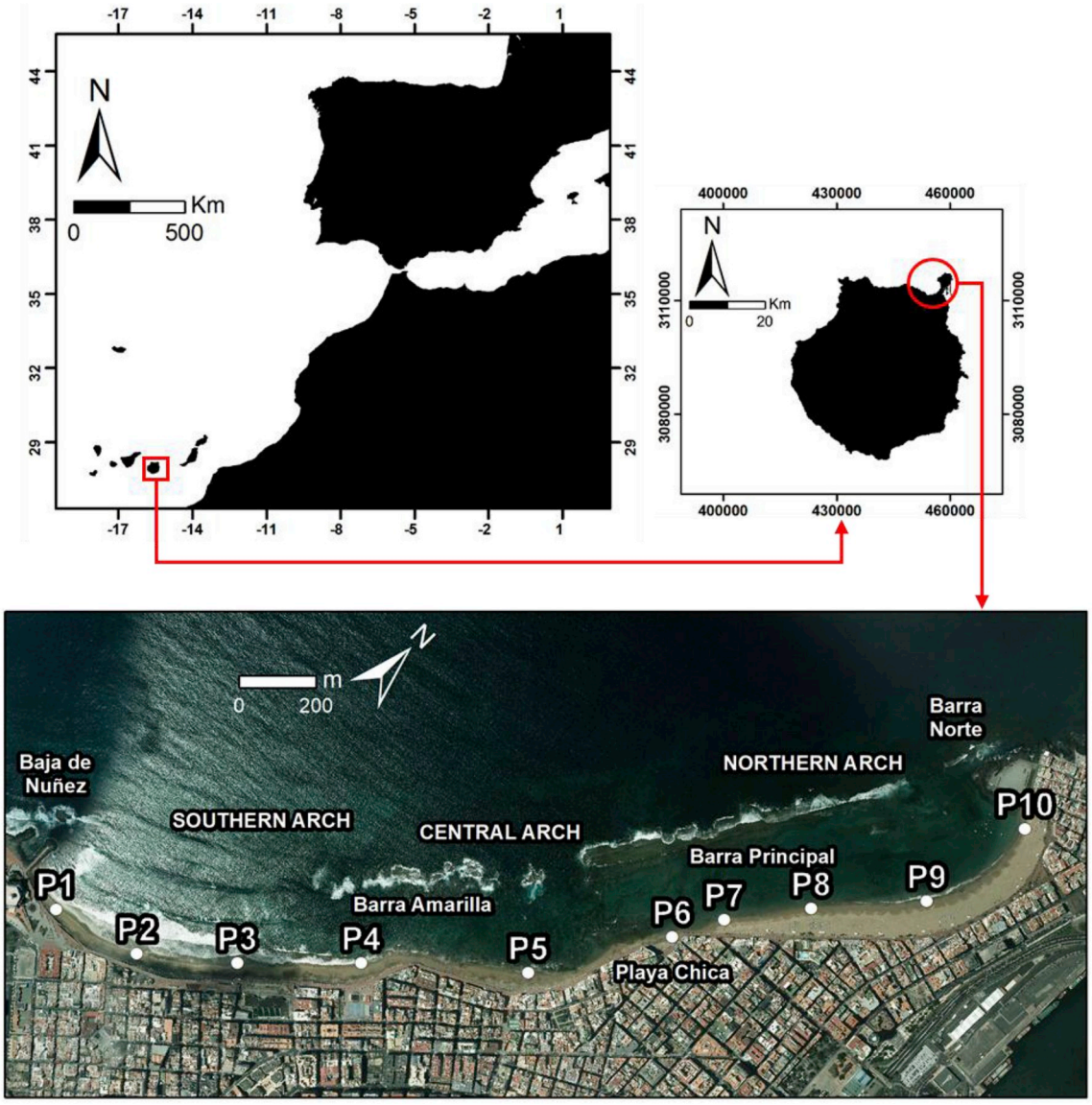

Fig. 1. Location, division and sampling points on Las Canteras beach. Coordinates are in the UTM system.

respectively, showed an enrichment in metal components (TiO_2, Fe_2O_3, MgO, V, Sc, Co and Cr) in the first one, while the organic sand (from north arch) presented higher amounts of K_2O, Na_2O, CaO, U, Sr, Ba, As and Th (Arnedo et al., 2013).

In front of the beach, there is a natural rocky bar offshore that emerges during low tide. This bar neither closes the whole beach nor is a complete block as shown in Fig. 1. Instead, it is fragmented in different sections with openings between them. The first part, located in the northern arch, presents an opening between the "Barra Norte" and the "Barra Principal." This part of the beach is completely protected against wave action. On the south part of the "Barra Principal," there is another opening, and the "Barra Amarilla" establishes the end of the protected part of the beach. The southern arch of the beach is completely exposed to the open ocean (Medina et al., 2006).

The sedimentary balance and dynamic of this beach has been studied, especially since building and development near the beach. Different studies (Alonso, 1993, 1994; 2005; Alonso and Vilas, 1996) indicate that the beach presents a seasonal variability with two different periods: erosion and accretion. According to these studies, erosional periods normally occur during intense storm events, so it is logical to expect them to occur during winter, while periods of accretion occur in summer. Furthermore, the beach has a different behaviour in its distinct parts due to the influence of many factors such as the presence of the natural offshore rocky bar and the type of sediments found on the different parts. During erosional periods, the southern arch loses a high amount of sediment that is transported longitudinally to the northern arch. During periods of accretion, sand from submerged sandbars is cross-transported to the beach so that the amount of sediment on the beach increases forming berms. Moreover, there are beach cusps formed on the northern arch during this period that can favor the presence of edge waves that generate longitudinal transport to the southern arch. Even though the sedimentary dynamic has long been studied in Las Canteras beach, there is still missing information about the origin and exchange of the sediment between the beach and the bay.

3. Material and methods

3.1. Samples collection and preparation

Ten points were selected in each campaign for sand sampling (Fig. 1). Four were located on the southern arch, one in the central arch, another one at Playa Chica, and the last four in the northern arch. In order to study any spatial and temporal variabilities on the radionuclides distribution along the beach, sand samples were taken monthly from September 2016 to August 2017 (120 samples in total). Moreover, pH, temperature and electroconductivity were measured at each sampling point. For this, a hole was made in the area of the square of each sampling point, digging until the water inside the soil emerged into the surface of the hole. Then pH, temperature and electroconductivity were measured from a sample of this water with a portable pH metre.

In order to consider the marine dynamic influence, samples were collected in the intertidal zone during low tide. For each one of them a square of 1 m^2 was drawn on the sand at each sampling point and, after mixing them *in situ*, samples were taken from the superficial sand from about 0 to 5 cm depth. Once in the laboratory, they were oven dried at 80 °C for 24 h. After this period, they were taken out of the oven and sieved through a 1 mm mesh size sieve to homogenise them. Finally, samples were kept inside PVC-trunk conical containers filled to 40 cm^3, then sealed with aluminium strips due to their impermeability to radon gas, and stored for approximately one month. This period was necessary to allow secular equilibrium between ^{226}Ra and ^{222}Rn and its short-lived progeny (as ^{214}Pb, used for determining ^{226}Ra).

3.2. Gamma emission analysis

The determination of radionuclides in sand samples by gamma spectrometry analysis was carried out using a Canberra Extended Range (XtRa) Germanium spectrometer, model GX3518, with 38% relative efficiency with respect to a 3″ x 3″ active area NaI (Tl) detector and nominal FWHM of 0.875 keV at 122 keV and 1.8 keV at 1.33 MeV. It works coupled to a Canberra DSA-1000 multichannel analyser with the software package Genie 2000. Efficiency calibration of the system was performed using the Canberra LabSOCS package based on the Monte Carlo method (Arnedo et al., 2017; G. Guerra et al., 2015, 2017). Calibration was verified using reference standards for IAEA RGK-1 (potassium sulfate), RGU-1 (uranium ore) and RGTh-1 (thorium ore). Energy calibration was carried out using a$^{155}Eu/^{22}Na$ (Canberra ISOXSRCE, 7F06-9/10138 series) and confirmed using the 1460.8 keV line of ^{40}K (IAEA RGK-1) (Arnedo et al., 2017).

The radionuclides of interest were determined from different photopeaks. ^{226}Ra was determined from the ^{214}Pb using the 351.9 keV emission line. The ^{210}Pb was directly measured using the emission line of 46.5 keV. The activity concentration of ^{232}Th was calculated from ^{228}Ac by the emission line of 911.2 keV. This emission line was also used to determine ^{228}Ra. Activity concentrations of ^{40}K and ^{137}Cs were directly measured using emission lines 1460.8 keV and 661.8 keV, respectively. The counting time for each sample was around 24 h. Finally, ^{210}Pb originates after the decay of ^{226}Ra, that produces ^{222}Rn, a 3.8 days half-life gas that partially diffuses into the atmosphere where it rapidly decays into ^{210}Pb. This fraction of ^{210}Pb is adsorbed to atmospheric aerosols and deposited as fallout over the earth's surface leading to unsupported or excess $^{210}Pb_{ex}$ (Al-Mur et al., 2017; Hülse and Bentley, 2012; Szmytkiewicz and Zalewska, 2014). The activity $^{210}Pb_{ex}$ was determined by the difference between the activity concentrations of ^{210}Pb and ^{226}Ra.

3.3. Granulometric analysis

Some aliquots were taken at each sampling point during the October 2016 campaign and a grain size analysis was carried out by dry sieving (Alveirinho Dias, 2004). Around 100 g of each sample were used. The aliquots were weighed and passed through five different sieves from 1 to 0.0625 mm at 1 ϕ intervals. Then, the portion retained on each sieve was weighed separately. The results were analysed by the GRADISTAT software (Blott and Pye, 2001).

3.4. Statistical analysis

A correlation analysis and two types of multivariate statistical analyses were performed to evaluate the spatial distribution of the activity concentration of ^{226}Ra, ^{232}Th, ^{40}K and $^{210}Pb_{ex}$, and its relations with other characteristics of the samples. The first multivariate analysis used was a cluster analysis (CA). This analysis identifies and classifies observations with similar characteristics within groups known as clusters. Observations in the same cluster are considered similar to each other and different to the observations in another cluster. Similarity is a measure of distance between any two individual variables (Ravisankar et al., 2014, 2015; Shaw, 2003) and, for this analysis, the Euclidian distance between the observations was used. Also, there are multiple types of CA and, in this work, the hierarchical CA was selected.

The second multivariate analysis was a principal component analysis (PCA) or empirical orthogonal functions (EOF) analysis (Thomson and Emery, 2014). This analysis takes a number of variables and converts them so that they can be more easily analysed, giving information about how variables relate with each other and identifying different groups of variables (Abramson et al., 2010; Guerrero et al., 2016; Thomson and Emery, 2014). According to literature, if the variance explained by the principal components is equal to or higher than 70%, the fitted principal component to the data is good (Ravisankar et al., 2014, 2015; Zhang et al., 2005).

4. Results and discussion

4.1. Activity concentrations

A Shapiro-Wilk normality test (Shapiro and Wilk, 1965) was performed on the activity concentration values of ^{226}Ra, ^{232}Th, ^{40}K and ^{210}Pb$_{ex}$ in each sampling point. The normality null hypothesis cannot be rejected at significance level of 0.05 for all activity concentrations samples except but the activity concentration of ^{210}Pb$_{ex}$ in sampling point P9 where normality behaviour cannot be rejected at level of significance 0.03 (p-value 0.033). The activity concentrations of ^{226}Ra, ^{232}Th, ^{40}K and ^{210}Pb$_{ex}$ for each sampling point are shown in the boxplots in Fig. 2. For ^{226}Ra, the activity concentration ranged between 5.4 ± 0.6 and 24.4 ± 1.4 Bq kg^{-1} with a mean value of 13.9 ± 0.9 Bq kg^{-1}; for ^{232}Th, it fluctuated between 6.4 ± 1.2 and 32.1 ± 2.0 Bq kg^{-1} with a mean value of 18.0 ± 1.6 Bq kg^{-1}; from 52 ± 6 to 810 ± 40 Bq kg^{-1} with a mean value of 429 ± 20 Bq kg^{-1} for ^{40}K; and between 12.4 ± 5.2 and 62.9 ± 6.4 Bq kg^{-1} with a mean value of 34.8 ± 5.5 Bq kg^{-1} for ^{210}Pb$_{ex}$.

A comparison of mean activity concentrations of ^{226}Ra, ^{232}Th and ^{40}K obtained in this work at Las Canteras beach, and those values referenced for other coastal sediments, is shown in Table 1. When comparing the results obtained in both studies at Las Canteras beach, it can be appreciated that although the activity concentration values given in this work are slightly higher, the results obtained in both works are similar. The values found for Las Canteras beach are also similar to others found for Xiamen Island in China (Huang et al., 2015), in sediments from the Cadiz Bay in Spain (Casas-Ruiz et al., 2012) and for values obtained in Tema Harbour in Ghana (Botwe et al., 2017), being slightly higher for ^{232}Th. In other places, like Iran (Abdi et al., 2008), the Oman Sea (Darabi-Golestan et al., 2017) and the Yangtze Estuary (Wang et al., 2017), the values found for the different radionuclides are all slightly higher, except for the case of the ^{40}K in Iran, which has a similar value to Las Canteras beach. In other places like Tamil Nadu in India (Punniyakotti and Ponnusamy, 2018) or in Henties Bay in Namibia (Onjefu et al., 2017), the variability is higher, with values for ^{226}Ra being one order of magnitude higher than the value obtained for Las Canteras beach. In Brazil, it is possible to find places like Bahia Coast (Veiga et al., 2006) where the values for ^{226}Ra and ^{232}Th are one order higher than the values found in this study, but the mean activity concentration for ^{40}K is one order of magnitude lower than the values obtained in Las Canteras beach. The activity concentration values obtained in Cumuruxatiba beach, on the south of Bahia in Brazil, (Vasconcelos et al., 2011), correspond to dark sand and show much higher values in comparison to everywhere else. These variations are probably due to the different minerals that can be found in the different places aforementioned, manifesting the variability in activity concentration in different places, which is related to the variation in the components of the sediments. Finally, when comparing with the worldwide values, ^{226}Ra and ^{232}Th are below the world mean, while ^{40}K is slightly higher than the mean value given by the United Nations Scientific Committee on the Effects of Atomic Radiation (UNSCEAR, 2000) for soil content.

4.2. Spatial analysis

When analysing the changes along the beach of the mean activity concentration for each radionuclide, an increase in ^{226}Ra, ^{232}Th and ^{40}K

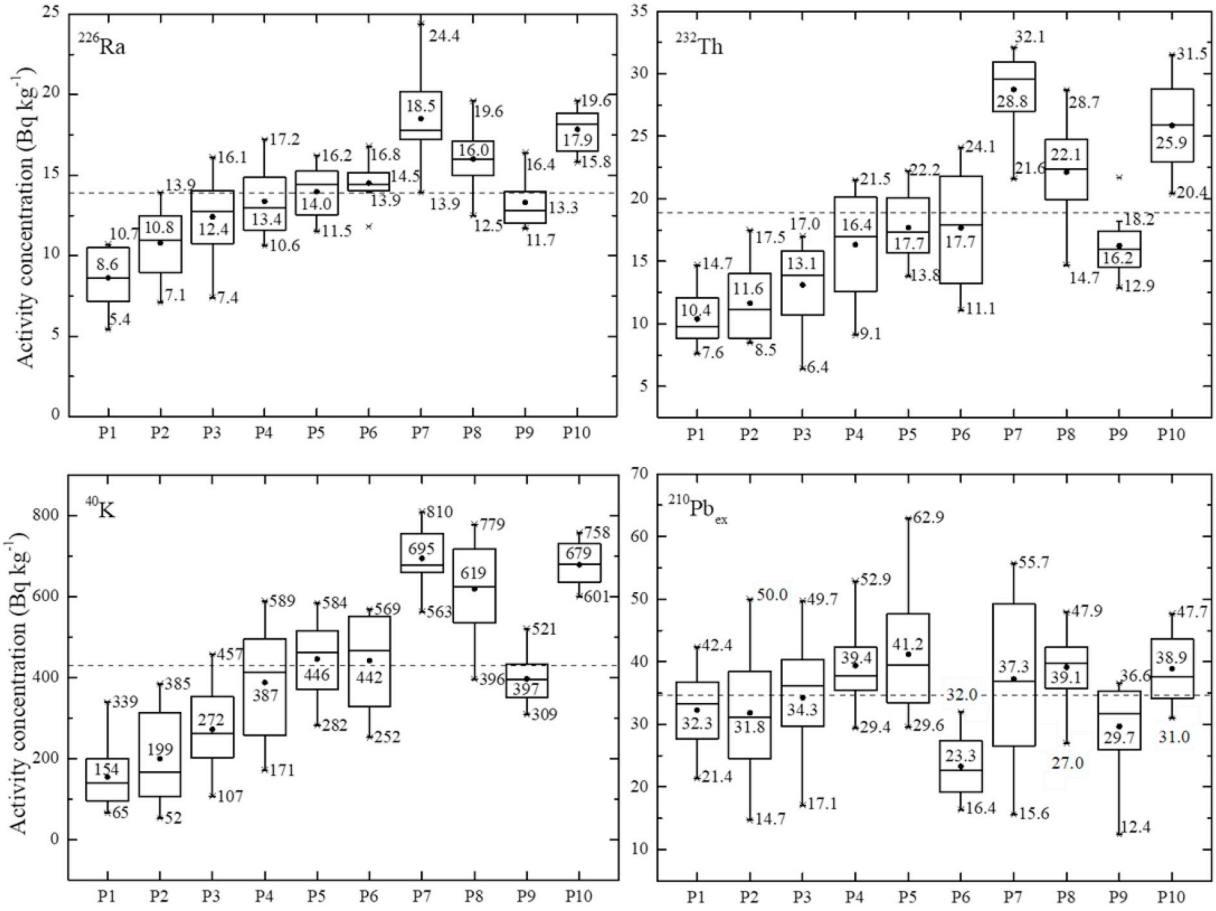

Fig. 2. Boxplots of the activity concentrations found for each sampling point for ^{226}Ra, ^{232}Th, ^{40}K and ^{210}Pb$_{ex}$. The dash line indicates the mean activity concentration value. The numbers that appear in each whisker correspond to the maximum and minimum activity concentration values. The number in the middle indicates the mean activity concentration value for each sampling point.

Table 1
Comparison of activity concentrations (Bq kg^{-1}) of ^{226}Ra, ^{232}Th and ^{40}K of Las Canteras beach sand and beach sand and marine sediments from coastal zones of other countries around the world.

Location	^{226}Ra		^{232}Th		^{40}K		Reference
	Range	Mean	Range	Mean	Range	Mean	
Las Canteras (Spain)	5.4–24.4	13.9	6.4–32	18.0	52–810	429	This work
Las Canteras (Spain)	7–19	14	7–25	15	83–629	390	Arnedo et al. (2013)
Xiamen Island (China)	7.9–25.7	14.6	6.7–41.4	10.9	197.4–421.3	396.4	Huang et al. (2015)
Cumuruxatiba (Brazil)	7050–8320	7810	17630–18450	17770	2220–3110	2660	Vasconcelos et al. (2011)
Persian Gulf (Iran)	17–48	35	15–45	26	146–500	395	Abdi et al. (2008)
Sediments of Cadiz Bay (Spain)	3–41	13	3–73	19	105–1342	451	Casas-Ruiz et al. (2012)
Oman sea (Arabic Gulf)	8–55	28	5–42	22	250–980	640	Darabi-Golestan et al. (2017)
Tema Harbour (Ghana)	–	14	–	30	–	325	Botwe et al. (2017)
Henties Bay (Namibia)	25.32–235.55	175.59	[1]BDL–77.99	40.17	222.39–482.16	349.66	Onjefu et al. (2017)
Bahia Coast (Brazil)	10–572	184	14–173	533	25–62	42	Veiga et al. (2006)
Tamil Nadu Coast (India)	[2]BDL–370.77	12.3	[2]BDL −3773.6	59.03	[2]BDL −525.9	197.03	Punniyakotti and Ponnusamy (2018)
Yangtze Estuary (China)	13.7–52.3	24.3	26.1–71.9	40.9	392–898	628	Wang et al. (2017)
Worldwide		32		45		420	UNSCEAR (2000)

BDL-Below detection limit: (1) not provided by authors, and (2) 2.22, 2.15, and 8.83 Bq kg^{-1} for ^{238}U, ^{232}Th, and ^{40}K, respectively.

is found from the southern to the northern arch of the beach. However, for $^{210}Pb_{ex}$ this variation is not present, being the value of activity concentration similar all along the beach except for P6 (Playa Chica). This seems to indicate that the spatial distribution of $^{210}Pb_{ex}$ is controlled by a different agent than the spatial distribution of ^{226}Ra, ^{232}Th and ^{40}K. Hence, the main dynamic agents contributing to the spatial distribution of these radionuclides could be related to wind for $^{210}Pb_{ex}$ (see section 3.2), and to waves and nearshore currents that transport the sediments for ^{226}Ra, ^{232}Th and ^{40}K. However, the distribution of the surface activity concentration of $^{210}Pb_{ex}$ is also influenced by the mixing or sediment accumulation rates (de Carvalho Gomes et al., 2009; Palanques et al., 2017; Szmytkiewicz and Zalewska, 2014). Thus, an analysis of ^{210}Pb activity concentration in sediment cores should be performed to better understand the agents that affect the spatial distribution of this element.

In addition to activity concentration values, other quantities were also measured. These include average grain size (ϕ), sorting, pH, conductivity (mS cm^{-1}), *in situ* temperature (°C) and bulk density (g cm^{-3}) for each sampling point (Table 2). Temperature (T), pH and conductivity (EC) show small variation along the beach, so a loss of radionuclides in a specific beach zone by chemical mobility between marine water and intertidal sand seems to be dismissed, even though a further analysis should be done.

A Shapiro-Wilk normality test (Shapiro and Wilk, 1965) was performed with a significance level of 0.05 to quantities aforementioned and mean activity concentration values of ^{226}Ra, ^{232}Th, ^{40}K and $^{210}Pb_{ex}$ (averaging for each point and for all the campaigns). The results indicate that almost all of them follow a normal distribution, since all of them have a p-value > 0.05, except for the grain size, which had a p-value of 0.02. Additionally, a performed correlation analysis is shown in Table 3. All coefficients correspond to the Pearson correlation coefficient (Ahlgren et al., 2003) except those relative to average grain size where Spearman correlation coefficients (Siegel and Castellan, 1988) were used. The p-value obtained for each correlation coefficient is also represented, being that correlation coefficients are statistically significant when p-values < 0.05. Moreover, a strong correlation was considered when p-value < 0.005.

Strong positive correlations appear between activity concentrations of ^{226}Ra, ^{232}Th and ^{40}K, and negative correlations between these activities and bulk densities of the samples. The temperature of the sample and the grain size also presented a moderate negative correlation with activity concentrations. Nevertheless, it is important to mention that temperature correlation could be related to the sampling hour, as samples with higher activity concentrations were systematically picked up earlier in the morning than samples from the part of the beach with less activity. Conductivity and pH did not present a significant correlation with the activity concentrations, which again suggest that the chemical mobility does not influence the variations of activity concentration of ^{226}Ra, ^{232}Th and ^{40}K. Thus, temperature, pH and conductivity were no longer considered for the rest of this study. In the case of $^{210}Pb_{ex}$, there is no significant correlation between this variable and the others. This seems to reinforce the idea that the main agents controlling the distribution of $^{210}Pb_{ex}$ are different than those controlling the distribution of the other radionuclides.

Once the descriptive statistic was established, the CA was performed by using activity concentrations of ^{226}Ra, ^{232}Th and ^{40}K. The dendrogram obtained from the cluster analysis is shown in Fig. 3. At a distance of 100, three different clusters appear; the first one with sampling points P1, P2 and P3; the second one with sampling points P4, P9, P5 and P6 and the third one with sampling points P7, P10 and P8 (Fig. 1). The classification obtained almost agrees with the geographical distribution of the sampling points except for the second group, where sampling

Table 2
Non-radioactive data and results obtained from granulometric analysis of the samples from Las Canteras beach. Mean values for pH, conductivity (EC), temperature (T), bulk density (ρ) of the sample, grain size in ϕ units, sorting, skewness and the classification of the samples depending on granulometric parameters are included.

Sampling point	pH	EC	T	ρ	Grain size	Sorting	Skewness	Classification		
		mS cm^{-1}	°C	g cm^{-3}	ϕ	ϕ	ϕ	Grain size	Sorting	Skewness
P1	8.09	54.03	21.25	2.030	2.532	0.414	0.141	Fine Sand	Well Sorted	Fine Skewed
P2	8.05	57.26	21.04	2.025	2.521	0.401	0.125	Fine Sand	Well Sorted	Fine Skewed
P3	8.17	57.72	20.82	1.945	2.449	0.450	−0.168	Fine Sand	Well Sorted	Coarse Skewed
P4	7.99	55.07	20.53	1.830	2.186	0.601	−0.230	Fine Sand	Moderately Well Sorted	Coarse Skewed
P5	8.13	56.92	20.42	1.812	2.304	0.623	−0.260	Fine Sand	Moderately Well Sorted	Coarse Skewed
P6	8.14	56.58	20.45	1.826	1.437	0.900	0.039	Medium Sand	Moderately Sorted	Symmetrical
P7	8.12	57.20	20.47	1.671	2.049	0.671	−0.211	Fine Sand	Moderately Well Sorted	Coarse Skewed
P8	8.24	56.80	20.30	1.712	2.409	0.470	−0.192	Fine Sand	Well Sorted	Coarse Skewed
P9	8.27	56.83	20.32	1.812	2.202	0.591	−0.268	Fine Sand	Moderately Well Sorted	Coarse Skewed
P10	8.13	55.95	20.60	1.668	2.194	0.586	−0.246	Fine Sand	Moderately Well Sorted	Coarse Skewed

Table 3
Correlation coefficients matrix of activity concentrations of ^{226}Ra, ^{232}Th, ^{40}K, ^{210}Pb$_{ex}$, pH, electroconductivity (EC), temperature (T), grain size in the ϕ scale, sorting and, bulk density (ρ) of samples. Correlation coefficients are shown in the bottom left diagonal and p-value at the top right diagonal in cursive.

	^{226}Ra	^{232}Th	^{40}K	^{210}Pb$_{ex}$	pH	EC	T	Size	Sorting	ρ
^{226}Ra	1	*0.000*	*0.000*	*0.312*	*0.489*	*0.294*	*0.017*	*0.016*	*0.143*	*0.000*
^{232}Th	0.972	1	*0.000*	*0.251*	*0.577*	*0.518*	*0.051*	*0.033*	*0.219*	*0.000*
^{40}K	0.979	0.980	1	*0.242*	*0.418*	*0.490*	*0.015*	*0.043*	*0.189*	*0.000*
^{210}Pb$_{ex}$	0.357	0.401	0.408	1	*0.615*	*0.903*	*0.603*	*0.960*	*0.326*	*0.245*
pH	0.249	0.201	0.289	−0.182	1	*0.200*	*0.161*	*0.855*	*0.935*	*0.366*
EC	0.369	0.233	0.248	−0.045	0.443	1	*0.258*	*0.651*	*0.776*	*0.567*
T	−0.730	−0.629	−0.736	−0.188	−0.479	−0.395	1	*0.187*	*0.071*	*0.005*
Size	−0.733	−0.673	−0.648	−0.018	−0.067	0.164	0.455	1	*0.000*	*0.077*
Sorting	0.498	0.427	0.452	−0.347	0.030	0.103	−0.592	−0.903	1	*0.149*
ρ	−0.960	−0.948	−0.985	−0.406	−0.321	−0.207	0.810	0.584	−0.492	1

*p = 0.000 corresponds to p < 0.005 (strong correlation).

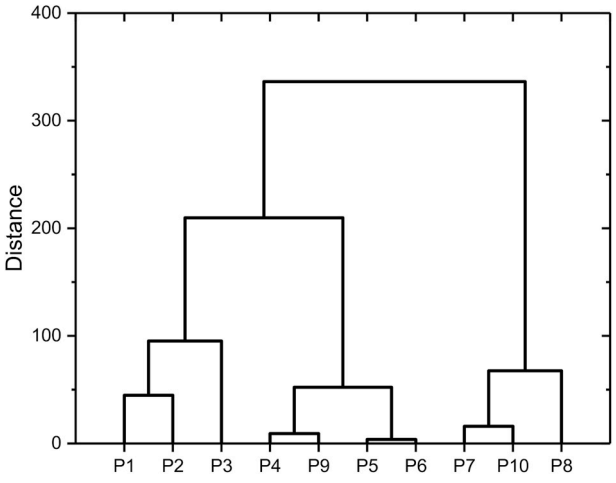

Fig. 3. Dendrogram showing clustering for the different sampling points based on their activity concentrations of ^{226}Ra, ^{232}Th and ^{40}K.

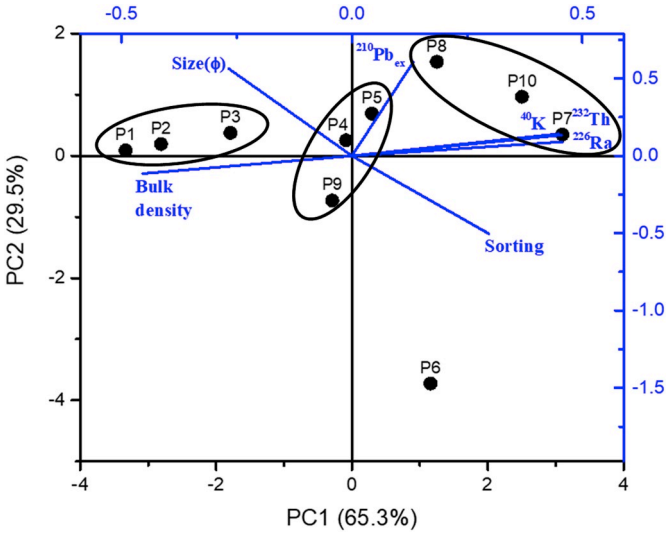

Fig. 4. Biplot of loading plot with the eigenvectors obtained for the grain size in the phi scale (Size ϕ), sorting, mass of the sample and activity concentrations of ^{226}Ra, ^{232}Th, ^{40}K and ^{210}Pb$_{ex}$ (blue axes) and scores of observations (black axes). (For interpretation of the references to colour in this figure legend, the reader is referred to the Web version of this article.)

points of the southern and northern arch are gathered together. The explanation for this, however, can be found, if the location of the sampling points is analysed. The first group of points, which will be referred to as Zone I, is located on the part of the beach without a natural offshore rocky bar, therefore, the beach is completely exposed to wave action. The second group, which will be referred to as Zone II, is the one where sampling points are located near the different openings in the bar described earlier. The last group, which will be referred to as Zone III, includes the sampling points that are located in the parts of the beach that are fully protected by the "Barra Norte" and the "Barra Principal" on the northern arch. Therefore, the presence of the distinct parts of the offshore rocky bar seems to be one of the main influences in the distribution of sediment transport and accumulation of radionuclides along the beach. This behaviour, referenced at least for Zone I and III by Alonso (1993), could be interpreted as a validation of the role of ^{226}Ra, ^{232}Th and ^{40}K as tracers of beach sedimentary dynamics.

PCA results are shown in the biplot in Fig. 4. In this biplot, the first two principal components (PC1 and PC2) are represented with an explanation of the total variance of 65.3 and 29.5%, respectively. On the one hand, activity concentrations of ^{226}Ra, ^{232}Th and ^{40}K present very small values of PC2, which means that the variance of these radionuclides is mostly explained by PC1 (Fig. 4 and Table 4). On the other hand, variance of ^{210}Pb$_{ex}$ is mainly explained by PC2 with factor loadings of 0.13 and 0.61, respectively (Table 4). This indicates that there is a higher correlation between the first three radionuclides, while ^{210}Pb$_{ex}$ follows a different pattern. This agrees with the results obtained from the correlation analysis and, again, reinforces the idea that radionuclide distribution along the beach is controlled by different agents and origins. Hence, the marine sedimentary dynamic could control ^{226}Ra, ^{232}Th and ^{40}K distribution while other causes, such as the aeolian sedimentary dynamic, would be the one controlling the distribution of ^{210}Pb$_{ex}$. In addition, the inverse correlation that exists between the grain size and the bulk density of the sample with the activity concentration of ^{226}Ra, ^{232}Th and ^{40}K is also represented. However, grain size values are given in the ϕ scale and this scale is opposite to metrics (Krumbein, 1934). Therefore, higher values in ϕ units indicate sediments are finer, thus, grain sizes and activity concentrations are directly correlated.

Moreover, Fig. 4 also exhibits the scores that the sampling locations

Table 4
Factor loadings of radiological variables on three significant principal components. Percentage of variance explained by each principal component and their cumulative percentage of total variance are also given.

Variables	PC1	PC2	PC3
^{226}Ra	0.46	0.09	−0.19
^{232}Th	0.45	0.14	−0.26
^{40}K	0.46	0.13	−0.18
^{210}Pb$_{ex}$	0.13	0.61	0.75
Size	−0.27	0.56	−0.21
Sorting	0.30	−0.50	0.51
Bulk density	−0.45	−0.11	0.05
% of Variance	65.3	29.5	3.9
Cumulative %	65.3	94.8	98.7

obtained on the PCA. These scores give an idea of how the observations are grouped and how they relate with the different variables. Results for ^{226}Ra, ^{232}Th and ^{40}K are mostly influenced by PC1, and three groups can be defined along this axis. The first group shows negative values of PC1 and includes sampling points P1, P2 and P3, all of them with the lowest activity concentration values of these radionuclides (Fig. 2). The second group includes all sampling points located around zero in the PC1 axis. These sampling points are P4, P5 and P9, all of them with intermediate activity concentrations. The third group refers to sampling points P7, P8 and P10. All of them present positive values in PC1 and their activity concentration values are the highest. The distribution of the sampling locations is slightly different from the one shown in Fig. 3, but it follows the same general pattern. Sampling points P1, P2 and P3 (Zone I) corresponds to negative values of PC1, sampling points P4, P5 and P9 (Zone II) are located close to zero values of PC1 and sampling stations P7, P8 and P10 (Zone III) show the higher values in PC1. The only exception is sampling point P6, located in a very particular place (mentioned in Section 2), so it could be under the influence of other variables.

Focusing on the second eigenvector (PC2), it mostly explains the variance associated with ^{210}Pb$_{ex}$, as was pointed out, perhaps mainly driven by aerosol dynamics. This component splits Zone II into two groups. On the one hand, the lowest values of PC2 correspond to sampling points P6 and P9, which present lower activity concentrations of this radionuclide (Fig. 2). Specifically, sampling P6 is in an area of the beach that is well protected against wind action, which could explain the lowest values of ^{210}Pb$_{ex}$ for that location (not only of Zone II, but for the entire beach). Opposite behaviour is followed by sampling stations P4 and P5, which show higher values of PC2 as a result of their ^{210}Pb$_{ex}$ activity concentrations higher than P6 and P9. However, the obtained values for P4 and P5 are of the same order as the ones obtained for ^{210}Pb$_{ex}$ in the rest of the beach. In other words, sampling points from Zone II scored mainly on PC2, while the rest scored mostly on PC1 (except P8 with similar scores in both PC1 and PC2). In view of the above, as well as PC1 and PC2 percentages of total variance, it could be said that the influence of ^{226}Ra, ^{232}Th and ^{40}K on sedimentary dynamics of Zones I and III is more of a determining factor than in Zone II where other dynamical agents could be considered.

Moreover, Zone I shows the lowest values in activity concentration of ^{226}Ra, ^{232}Th and ^{40}K, as well as in grain size (highest in ϕ units) and the highest in bulk density. Sediments in this area are fine sands (0.177 mm average size) with a high proportion of metal components. Bulk density values respond to the sediment density, and therefore, to their composition. In this area, most common sediments are heavy-metal oxides (mostly magnetite and ilmenite) and pyroxenes (Alonso, 1993; Alonso and Pérez Torrado, 1992), whose densities are 5.18, 4.75 and 3.3 g cm^{-3} for magnetite, ilmenite and pyroxenes, respectively. On the other hand, the most common material at the northern sector of the beach (sampling points P7, P8 and P10, Zone III) are bioclastic sands (0.215 mm average size) rich in calcite and aragonite with a density of 2.75 and 2.93 g cm^{-3}, respectively, and, according to what was stated in Section 2, with higher proportions of K_2O, as well as of Th and U, than Zone I. This agrees with the fact that samples collected from Zone I, where the mineral composition is dominant, shows lower activities of ^{232}Th, ^{226}Ra and ^{40}K and higher bulk density. The scores obtained by samples from Zone III, samples of more calcareous and organic origin, are opposite to those from Zone I, pointing out that these samples have lower mass and higher activity concentration.

4.3. Temporal analysis

Dai et al. (2011) suggested the use of the ratio ^{226}Ra/^{228}Ra as a tracer for erosion and accretion periods in a marine environment. According to them, ^{228}Ra and ^{226}Ra are more present in the crystal framework of clay minerals, but the carbonate and exchangeable phases contain more ^{228}Ra. Thus, accretion or erosion periods could be measured by a change in the ratio between ^{226}Ra and ^{228}Ra. Hence, during accretion periods, the input of ^{228}Ra would be higher and the value of the ratio would be less than 1 (i.e., the natural ratio of ^{232}Th/^{238}U was assumed); a value higher than 1 would indicate an erosional period. Some crystals from clay minerals and zeolites have been found in the north of Las Canteras beach, (Mangas and Julià-Miralles, 2015). Therefore, this ratio could be used to perform the temporal analysis. Moreover, as the spatial analysis presented three different sectors along the beach, that could be related to different dynamic behaviour, the analysis was performed in each one of these zones.

Fig. 5 shows the results after applying the ^{226}Ra/^{228}Ra ratio to the three zones of the beach. Zone III is the area that is fully protected by the natural offshore rocky bar, and all values are lower than 1. This would indicate that Zone III presented a constant accretion during the whole study period. Moreover, from March 2017 to August 2017, there seems to be a decrease in the ratio values, compared to the values obtained in October and December 2016, suggesting a more intense accretion of sediments during the first mentioned period.

Zone II is the part of the beach located opposite to the openings of the calcarenitic bar, so it is likely to have a more complex dynamic. Two periods could be differentiated. The first one occurs from September 2016 through February 2017, when values of ^{226}Ra/^{228}Ra ratio were around 1, indicating small changes in sediment volume. The second period occurs from March through August 2017, and the ratio is clearly less than 1, suggesting accretion, which should be stronger in July and August.

In Zone I, September 2016 and February 2017 present ^{226}Ra/^{228}Ra ratios around 1.25, indicating strong erosion, while October 2016 and July 2017 show ^{226}Ra/^{228}Ra ratios around 0.75, indicating strong deposition. The rest of the months have values around 1. The strong variability suggests that the processes of erosion and accretion in this area are stronger than in the others, involving large amount of sediments that are moved away in the case of erosion and accumulated in the case of accretion.

Unfortunately, we do not have data of volume changes along the beach for the same study period, which could be used to confirm or discard what has been inferred from ^{226}Ra/^{228}Ra ratios. Nevertheless, previous studies in this beach point out that Zone III presents a clear accumulative trend in the long term, Zone II shows much lower volume changes because of the presence of a rocky substratum that is present all along this area, and Zone I presents a very strong seasonal variability, consisting of erosive periods during winter followed by strong accretion during summer (Alonso, 1993; Alonso and Vilas, 1996). Obtained ratios of ^{226}Ra/^{228}Ra seem to confirm the accretion at Zone III, certain seasonal changes at Zone II and strong changes at Zone I. However, further studies with longer time series are necessary to better understand the temporal variability of the environmental radioactivity of the beach, and to get a better correlation with the sedimentary dynamics at this beach. In addition to testing whether the decision value for the ^{226}Ra/^{228}Ra ratio is 1 or somewhat lower, depends on more adequate average natural ^{232}Th/^{238}U ratio in Las Canteras.

5. Conclusions

The analysis of spatial and temporal variations of activity concentrations of ^{226}Ra, ^{232}Th and ^{40}K of intertidal sand samples seems to indicate its feasibility to trace different characteristic processes of the sedimentary dynamics at Las Canteras beach (which involves typical dynamics of both a wave action protected beach and one open to this action).

A CA and a PCA were carried out to evaluate the spatial variability of activity concentrations, showing that sampling points are grouped in three zones with activity concentration values conditioned by the morphology of the natural offshore rocky bar. Thus, the sampling points that are not influenced by the rocky bar correspond to Zone I and present the lowest activity concentrations of ^{226}Ra, ^{232}Th and ^{40}K. Zone II includes sampling points that are located near the different openings in the

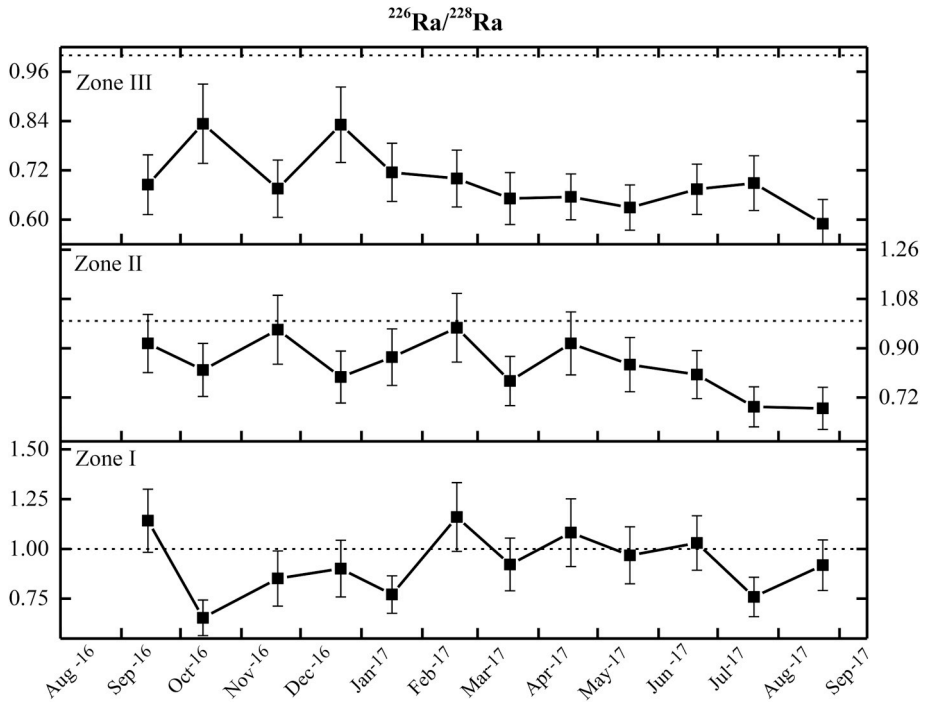

Fig. 5. Mean $^{226}Ra/^{228}Ra$ ratios for each campaign in each zone of Las Canteras beach. Dash lines correspond to value 1 for the ratio.

bar. Being that this zone is partially protected from wave action, it presents intermediate values of activity concentrations. Finally, Zone III refers to sampling points that are in parts of the beach that are fully protected by the "Barra Norte" and "Barra Principal" on the northern arch. Sampling points in this area present the highest values in activity concentration. Therefore, it seems viable that ^{226}Ra, ^{232}Th and ^{40}K can be used as tracers of the distribution of sediments along the beach based on the different marine dynamics related to the morphology of the offshore rocky bar at Las Canteras beach.

The temporal analysis was performed by mean of the ratio $^{226}Ra/^{228}Ra$ in order to evaluate erosion and accretion of sediment periods along the beach. The results suggest that Zones I and II could be affected by either erosion or accretion, while Zone III shows a steady accretionary process, which agrees with previous studies at Las Canteras beach. However, a longer-term study would be necessary to better understand the relation between temporal variability of the environmental radioactivity and beach erosion/accretion periods.

Finally, the use of these natural radionuclides as tracers of the different sedimentary dynamics of Las Canteras beach could provide useful information for beach anthropogenic management, as well as to control and manage any spills that may occur near the beach. Moreover, this study could easily be extended to the management of other beaches of similar sedimentary dynamics.

Declaration of competing interest

The authors declare that they have no known competing financial interests or personal relationships that could have appeared to influence the work reported in this paper.

References

Abdi, M.R., Kamali, M., Vaezifar, S., 2008. Distribution of radioactive pollution of ^{238}U, ^{232}Th, ^{40}K and ^{137}Cs in northwestern coasts of Persian Gulf, Iran. Mar. Pollut. Bull. 56, 751–757. https://doi.org/10.1016/j.marpolbul.2007.12.010.

Abramson, L., Lee, C., Liu, Z., Wakeham, S., Szlosek, J., 2010. Exchange between suspended and sinking particles in the northwest Mediterranean as inferred from the organic composition of *in situ* pump and sediment trap samples. Limnol. Oceanogr. 55, 725–739. https://doi.org/10.4319/lo.2009.55.2.0725.

Ahlgren, P., Jarneving, B., Rousseau, R., 2003. Requirements for a cocitation similarity measure, with special reference to Pearson's correlation coefficient. J. Assoc. Inf. Sci. Technol. 54, 550–560. https://doi.org/10.1002/asi.10242.

Al-Mur, B.A., Quicksall, A.N., Kaste, J.M., 2017. Determination of sedimentation, diffusion, and mixing rates in coastal sediments of the eastern Red Sea via natural and anthropogenic fallout radionuclides. Mar. Pollut. Bull. 122, 456–463. https://doi.org/10.1016/j.marpolbul.2017.05.054.

Alonso, I., 1993. Procesos sedimentarios en la playa de Las Canteras (Gran Canaria). Universidad de Las Palmas de Gran Canaria.

Alonso, I., 1994. Spatial beach morphodynamics. An example from Canary Islands, Spain. Litoral, 94, 169–183.

Alonso, I., 2005. Costa Norte: playa de las Canteras. In: Hernández, L., Alonso, I., Mangas, J., Yanes, A. (Eds.), Tendencias Actuales En Geomorfología Litoral. Universidad de Las Palmas de Gran Canaria, La Palmas de Gran Canaria, pp. 219–238.

Alonso, I., Pérez Torrado, F.J., 1992. Estudio sedimentológico de la playa de Las Canteras (Gran Canaria). Datos preliminares. III Congreso Geológico España tomo 2, 131–135.

Alonso, I., Vilas, F., 1996. Variabilidad sedimentaria en la playa de Las Canteras (Gran Canaria). Geogaceta 20, 428–430.

Alveirinho Dias, J., 2004. A análise sedimentar e o conhecimento dos sistemas marinhos: uma introdução à oceanografia geológica, first ed. Universidade do Algarve, Faro, p. 84.

Arnedo, M.A., Rubiano, J.G., Alonso, H., Tejera, A., González, A., González, J., Gil, J.M., Rodríguez, R., Martel, P., Bolivar, J.P., 2017. Mapping natural radioactivity of soils in the eastern Canary Islands. J. Environ. Radioact. 166, 242–258. https://doi.org/10.1016/j.jenvrad.2016.07.010.

Arnedo, M.A., Tejera, A., Rubiano, J.G., Alonso, H., Gil, J.M., Rodríguez, R., Martel, P., 2013. Natural radioactivity measurements of beach sands in gran Canaria, Canary Islands (Spain). Radiat. Prot. Dosim. 156, 75–86. https://doi.org/10.1093/rpd/nct044.

Blott, S.J., Pye, K., 2001. Technical communication Gradistat : a grain size distribution and statistics package for the analysis of unconsolidated sediments. Earth Surf. Process. Landforms 26, 1237–1248. https://doi.org/10.1002/esp.261.

Botwe, B.O., Schirone, A., Delbono, I., Barsanti, M., Delfanti, R., Kelderman, P., Nyarko, E., Lens, P.N.L., 2017. Radioactivity concentrations and their radiological significance in sediments of the Tema Harbour (Greater Accra, Ghana). J. Radiat. Res. Appl. Sci. 10, 63–71. https://doi.org/10.1016/j.jrras.2016.12.002.

Carvalho, F.M., da Costa Lauria, D., Araújo Ribeiro, F.C., Tonelli Fonseca, R., da Silva Peres, S., Falcão Martins, N.S., 2016. Natural and man-made radionuclides in sediments of an inlet in Rio de Janeiro State, Brazil. Mar. Pollut. Bull. 107, 269–276. https://doi.org/10.1016/j.marpolbul.2016.03.059.

Casas-Ruiz, M., Ligero, R.A., Barbero, L., 2012. Estimation of annual effective dose due to natural and man-made radionuclides in the metropolitan area of the Bay of Cadiz (SW of Spain). Radiat. Prot. Dosim. 150, 60–70. https://doi.org/10.1093/rpd/ncr360.

Dai, Z.J., Du, J.Z., Chu, A., Zhang, X.L., 2011. Sediment characteristics in the north branch of the Yangtze estuary based on radioisotope tracers. Environ. Earth Sci. 62, 1629–1634. https://doi.org/10.1007/s12665-010-0647-7.

Darabi-Golestan, F., Hezarkhani, A., Zare, M.R., 2017. Assessment of ^{226}Ra, ^{238}U, ^{232}Th, ^{137}Cs and ^{40}K activities from the northern coastline of Oman Sea (water and sediments). Mar. Pollut. Bull. 118, 197–205. https://doi.org/10.1016/j.marpolbul.2017.02.064.

de Carvalho Gomes, F., Godoy, J.M., Godoy, M.L.D.P., Lara de Carvalho, Z., Tadeu Lopes, R., Sanchez-Cabeza, J.A., Drude de Lacerda, L., Cesar Wasserman, J., 2009. Metal concentrations, fluxes, inventories and chronologies in sediments from Sepetiba and Ribeira Bays: a comparative study. Mar. Pollut. Bull. 59, 123–133. https://doi.org/10.1016/j.marpolbul.2009.03.015.

Du, J., Wu, Y., Huang, D., Zhang, J., 2010. Use of ^{7}Be, ^{210}Pb and ^{137}Cs tracers to the transport of surface sediments of the Changjiang Estuary, China. J. Mar. Syst. 82, 286–294. https://doi.org/10.1016/j.jmarsys.2010.06.003.

Fares, S., 2017. Measurements of natural radioactivity level in black sand and sediment samples of the Temsah Lake beach in Suez Canal region in Egypt. J. Radiat. Res. Appl. Sci. 10, 194–203. https://doi.org/10.1016/j.jrras.2017.04.007.

Ghosal, S., Agrahari, S., Guin, R., Sengupta, D., 2017. Implications of modelled radioactivity measurements along coastal. Estuar. Coast Shelf Sci. 184, 83–89.

Guerra, J.G., Rubiano, J.G., Winter, G., Guerra, A.G., Alonso, H., Arnedo, M.A., Tejera, A., Gil, J.M., Rodríguez, R., Martel, P., Bolivar, J.P., 2015. A simple methodology for characterization of germanium coaxial detectors by using Monte Carlo simulation and evolutionary algorithms. J. Environ. Radioact. 149, 8–18. https://doi.org/10.1016/j.jenvrad.2015.06.017.

Guerra, J.G., Rubiano, J.G., Winter, G., Guerra, A.G., Alonso, H., Arnedo, M.A., Tejera, A., Martel, P., Bolivar, J.P., 2017. Computational characterization of HPGe detectors usable for a wide variety of source geometries by using Monte Carlo simulation and a multi-objective evolutionary algorithm. Nucl. Instrum. Methods Phys. Res., Sect. A: Accel. Spectrom. Detect. Assoc. Equip. 858, 113–122. https://doi.org/10.1016/j.nima.2017.02.087.

Guerrero, J.L., Vallejos, Á., Cerón, J.C., Sánchez-Martos, F., Pulido-Bosch, A., Bolívar, J. P., 2016. U-isotopes and ^{226}Ra as tracers of hydrogeochemical processes in carbonated karst aquifers from arid areas. J. Environ. Radioact. 158–159, 9–20. https://doi.org/10.1016/j.jenvrad.2016.03.015.

Gulin, S.B., Gulina, L.V., Sidorov, I.G., Proskurnin, V.Y., Duka, M.S., Moseichenko, I.N., Rodina, E.A., 2014. ^{40}K in the Black Sea: a proxy to estimate biogenic sedimentation. J. Environ. Radioact. 54, 231–242. https://doi.org/10.1016/j.jenvrad.2014.02.011.

Huang, Y., Lu, X., Ding, X., Feng, T., 2015. Natural radioactivity level in beach sand along the coast of Xiamen Island, China. Mar. Pollut. Bull. 91, 357–361. https://doi.org/10.1016/j.marpolbul.2014.11.046.

Hülse, P., Bentley, S.J., 2012. A ^{210}Pb sediment budget and granulometric record of sediment fluxes in a subarctic deltaic system: the Great Whale River, Canada. Estuar. Coast Shelf Sci. 109, 41–52. https://doi.org/10.1016/j.ecss.2012.05.019.

Korkulu, Z., Özkan, N., 2013. Determination of natural radioactivity levels of beach sand samples in the black sea coast of Kocaeli (Turkey). Radiat. Phys. Chem. 88, 27–31. https://doi.org/10.1016/j.radphyschem.2013.03.022.

Krumbein, W.C., 1934. Size frequency distributions of sediments. J. Sediment. Res. 4, 65–77. https://doi.org/10.1306/D4268EB9-2B26-11D7-8648000102C1865D.

Mahu, E., Nyarko, E., Hulme, S., Swarzenski, P., Asiedu, D.K., Coale, K.H., 2016. Geochronology and historical deposition of trace metals in three tropical estuaries in the Gulf of Guinea. Estuar. Coast Shelf Sci. 177, 31–40. https://doi.org/10.1016/j.ecss.2016.05.007.

Malain, D., Regan, P.H., Bradley, D.A., Matthews, M., Al-Sulaiti, H.A., Santawamaitre, T., 2012. An evaluation of the natural radioactivity in Andaman beach sand samples of Thailand after the 2004 tsunami. Appl. Radat. Isot. 70, 1467–1474. https://doi.org/10.1016/j.apradiso.2012.04.017.

Mangas, J., Julià-Miralles, M., 2015. Geomorfología y naturaleza de las bajas submareales de Bajo Fernando, Los Roquerillos y La Zabala (NE de Gran Canaria). Geotemas 15, 37–40.

Medina, R., Bastón, S., Cánovas, V., Torres, A., Luque, Á., Alonso, I., Sánchez, I., Ortega, A., Rodríguez, S., Martín, J.A., 2006. Estudio integral de la playa de Las Canteras. Technical Report Dirección General de Costas.

Oguri, K., Harada, N., Tadai, O., 2012. Excess ^{210}Pb and ^{137}Cs concentrations, mass accumulation rates, and sedimentary processes on the Bering Sea continental shelf. Deep-Sea Res 193–204. https://doi.org/10.1016/j.dsr2.2011.03.007 part II 61–64.

Onjefu, S.A., Taole, S.H., Kgabi, N.A., Grant, C., Antoine, J., 2017. Assessment of natural radionuclide distribution in shore sediment samples collected from the North Dune beach, Henties Bay, Namibia. J. Radiat. Res. Appl. Sci. 10, 301–306. https://doi.org/10.1016/j.jrras.2017.07.003.

Palanques, A., Lopez, L., Guillén, J., Puig, P., Masqué, P., 2017. Decline of trace metal pollution in the bottom sediments of the Barcelona City continental shelf (NW Mediterranean). Sci. Total Environ. 579, 755–767. https://doi.org/10.1016/j.scitotenv.2016.11.031.

Pappa, F.K., Tsabaris, C., Ioannidou, A., Patiris, D.L., Kaberi, H., Pashalidis, I., Eleftheriou, G., Androulakaki, E.G., Vlastou, R., 2016. Radioactivity and metal concentrations in marine sediments associated with mining activities in Ierissos Gulf, North Aegean Sea, Greece. Appl. Radiat. Isot. 116, 22–33. https://doi.org/10.1016/j.apradiso.2016.07.006.

Punniyakotti, J., Ponnusamy, V., 2018. Environmental radiation and potential ecological risk levels in the intertidal zone of southern region of Tamil Nadu coast (HBRAs), India. Mar. Pollut. Bull. 127, 377–386. https://doi.org/10.1016/j.marpolbul.2017.11.026.

Ravisankar, R., Chandramohan, J., Chandrasekaran, A., Prince Prakash Jebakumar, J., Vijayalakshmi, I., Vijayagopal, P., Venkatraman, B., 2015. Assessments of radioactivity concentration of natural radionuclides and radiological hazard indices in sediment samples from the East coast of Tamilnadu, India with statistical approach. Mar. Pollut. Bull. 97, 419–430. https://doi.org/10.1016/j.marpolbul.2015.05.058.

Ravisankar, R., Sivakumar, S., Chandrasekaran, A., Prince Prakash Jebakumar, J., Vijayalakshmi, I., Vijayagopal, P., Venkatraman, B., 2014. Spatial distribution of gamma radioactivity levels and radiological hazard indices in the East Coastal sediments of Tamilnadu, India with statistical approach. Radiat. Phys. Chem. 103, 89–98. https://doi.org/10.1016/j.radphyschem.2014.05.037.

Renfro, A.A., Cochran, J.K., Hirschberg, D.J., Bokuniewicz, H.J., Goodbred Jr., S.L., 2016. The sediment budget of an urban coastal lagoon (Jamaica Bay, NY) determined using ^{234}Th and ^{210}Pb. Estuar. Coast Shelf Sci. 180, 136–149.

Shapiro, S.S., Wilk, M.B., 1965. An analysis of variance test for normality (complete samples). Biometrika 52, 591–611. https://doi.org/10.2307/2333709.

Shaw, P.J., 2003. Multivariate Statistics for the Environmental Science, First. ed. Hodder Headline Group, London, p. 244.

Shuaibu, H.K., Khandaker, M.U., Alrefae, T., Bradley, D.A., 2017. Assessment of natural radioactivity and gamma-ray dose in monazite rich black Sand Beach of Penang Island, Malaysia. Mar. Pollut. Bull. 119, 423–428. https://doi.org/10.1016/j.marpolbul.2017.03.026.

Siegel, S., Castellan, J.N., 1988. Nonparametric Statistics for the Behavioural Science, Second. McGraw-Hill, New York, p. 399.

Suresh Gandhi, M., Ravisankar, R., Rajalakshmi, A., Sivakumar, S., Chandrasekaran, A., Pream Anand, D., 2014. Measurements of natural gamma radiation in beach sediments of north east coast of Tamilnadu, India by gamma ray spectrometry with multivariate statistical approach. J. Radiat. Res. Appl. Sci. 7, 7–17. https://doi.org/10.1016/j.jrras.2013.11.001.

Szmytkiewicz, A., Zalewska, T., 2014. Sediment deposition and accumulation rates determined by sediment trap and ^{210}Pb isotope methods in the outer puck bay (Baltic Sea). Oceanologia 56, 85–106. https://doi.org/10.5697/oc.56-1.085.

Thomson, R.E., Emery, W.J., 2014. The spatial analyses of data fields. In: Thomson, R.E., Emery, W.J. (Eds.), Data Analysis Methods in Physical Oceanography. Elsevier Science, Amsterdam, pp. 335–340. https://doi.org/10.1017/CBO9781107415324.004.

UNSCEAR, 2000. Sources and Effects of Ionizing Radiation. Report of the United Nations Scientific Committee on the Effects of Atomic Radiation to the General Assembly, with Scientific Annexes. United Nations, New York.

Vasconcelos, D.C., Pereira, C., Oliveira, A.H., Santos, T.O., Rocha, Z., Menezes, M.Â.de B. C., 2011. Determination of natural radioactivity in beach sand in the extreme south of Bahia, Brazil, using gamma spectrometry. Radiat. Prot. Environ. 34, 178–184. https://doi.org/10.4103/0972-0464.101714.

Veiga, R., Sanches, N., Anjos, R.M., Macario, K., Bastos, J., Iguatemy, M., Aguiar, J.G., Santos, A.M.A., Mosquera, B., Carvalho, C., Filho, M.B., Umisedo, N.K., 2006. Measurement of natural radioactivity in Brazilian beach sands. Radiat. Meas. 41, 189–196. https://doi.org/10.1016/j.radmeas.2005.05.001.

Wang, J., Du, J., Bi, Q., 2017. Natural radioactivity assessment of surface sediments in the Yangtze Estuary. Mar. Pollut. Bull. 114, 602–608. https://doi.org/10.1016/j.marpolbul.2016.09.040.

Woszczyk, M., Poreba, G., Malinowski, Ł., 2017. ^{210}Pb, ^{137}Cs and ^{7}Be in the sediments of coastal lakes on the Polish coast: implications for sedimentary processes. J. Environ. Radioact. 169 (170), 174–185. https://doi.org/10.1016/j.jenvrad.2017.01.015.

Zhang, H., Lu, Y., Dawson, R.W., Shi, Y., Wang, T., 2005. Classification and ordination of DDT and HCH in soil samples from the Guanting Reservoir, China. Chemosphere 60, 762–769. https://doi.org/10.1016/j.chemosphere.2005.04.023.